

# A photofuel cell comprising titanium oxide and silver(I/O) photocatalysts for use of acidic water as a fuel†

Cite this: *Chem. Commun.*, 2014, 50, 3067

Received 9th January 2014,  
Accepted 4th February 2014

DOI: 10.1039/c4cc00194j

www.rsc.org/chemcomm

Yuta Ogura,<sup>a</sup> Seiji Okamoto,<sup>a</sup> Takaomi Itoi,<sup>b</sup> Yukiko Fujishima,<sup>a,c</sup> Yusuke Yoshida<sup>a</sup> and Yasuo Izumi<sup>\*a</sup>

**A photofuel cell comprising two photocatalysts TiO<sub>2</sub> and Ag–TiO<sub>2</sub> is demonstrated. The open circuit voltage, short circuit current, and maximum electric power of the PFC were 1.59 V, 74 μA, and 14 μW, respectively. The electron flow was rectified due to the Schottky barrier between TiO<sub>2</sub> and Ag nanoparticles.**

Fossil fuels have been utilized as an essential energy source for industrialization. The industrial CO<sub>2</sub> emissions have led to an increase in the level of atmospheric CO<sub>2</sub> concentration (400 ppm), and the effects of this increase on global warming cannot be underestimated. The development of renewable energy as a replacement for fossil fuels has been slow.<sup>1,2</sup> Among the renewable energies, solar energy has the greatest potential. Although silicon solar cells (Si SC) have been commercialized, the technology that can convert solar energy to electricity often needs subsidies to spread more widely.<sup>3</sup> Other types of SCs<sup>4</sup> and fuel cells (FCs) that use hydrogen fuel<sup>5</sup> potentially obtained using solar energy<sup>6</sup> have been extensively investigated. However, all the requisites (sustainability, durability, and an electromotive force of 1–3 V per cell) have not been fully satisfied.

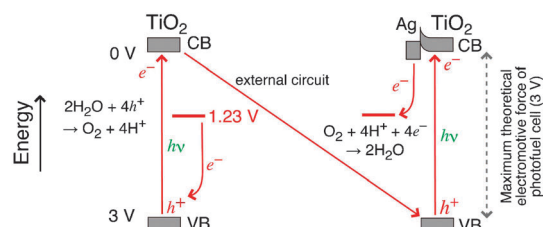
In this study, we demonstrate a new device: a photofuel cell (PFC) utilizing two photocatalysts TiO<sub>2</sub> and silver(I/O)-doped TiO<sub>2</sub> on an electrode film, both immersed in acidic solutions separated by a proton-conducting polymer (PCP). The cell mechanism of redox reactions over the photocatalysts and the flow of electrons and protons in the cell facilitates a theoretical electromotive force of 3 V if some reasons (charge recombination in electrodes, electrons confined in Ag, and reverse electron flow from cathode to anode) for overvoltage are not taken into account. Moreover, the use of acidic water as a fuel is inexpensive and sustainable.

<sup>a</sup> Department of Chemistry, Graduate School of Science, Chiba University, Yayoi 1-33, Inage-ku, Chiba 263-8522, Japan. E-mail: yizumi@faculty.chiba-u.jp; Fax: +81-43-290-2783; Tel: +81-43-290-3696

<sup>b</sup> Department of Mechanical Engineering, Graduate School of Engineering, Chiba University, Yayoi 1-33, Inage-ku, Chiba 263-8522, Japan

<sup>c</sup> Department of Chemistry, Faculty of Science, Tokyo University of Science, Kagurazaka 1-3, Shinjuku-ku, Tokyo 163-8601, Japan

† Electronic supplementary information (ESI) available: The derivation of eqn (2) for photocurrents of PFC, experimental methods, EXAFS curve-fit results, CV peak positions, and supplementary EM images. See DOI: 10.1039/c4cc00194j



Scheme 1 The energy diagram of PFC comprising two photocatalyst electrodes.

The concept of PFC is shown in Scheme 1. The band gap values for anatase- and rutile-type TiO<sub>2</sub> are 3.2 and 3.0 eV,<sup>7,8</sup> respectively, and charges (holes, electrons) are separated by UV (and minor visible) light irradiation. The holes in TiO<sub>2</sub> diffused to the surface to photooxidize water, while the electrons in Ag–TiO<sub>2</sub> diffused to the TiO<sub>2</sub> surface and then to Ag nanoparticles to photoreduce O<sub>2</sub> molecules. Thus, in the cell, electron flow from the conduction band (CB) of TiO<sub>2</sub> to the valence band (VB) of Ag–TiO<sub>2</sub> is obtained. Because the Schottky barrier is formed at the interface between TiO<sub>2</sub> and Ag nanoparticles, the electron flow from TiO<sub>2</sub> to Ag is rectified.

This concept of PFC comprising two photoelectrodes is different from FCs comprising a photoanode and a conventional cathode such as Pt–carbon,<sup>9–15</sup> dye-sensitized SCs comprising a dye on a semiconductor and a conventional cathode,<sup>3</sup> and combination of two photocatalysts separated by a PCP film to produce O<sub>2</sub> and H<sub>2</sub> independently from water.<sup>16–18</sup> Recently, a PFC comprising WO<sub>3</sub> photoanode and a Cu<sub>2</sub>O/Cu photocathode was reported using organic dyes as a fuel.<sup>19</sup> In this study, (acidic) water is used as a fuel<sup>15</sup> and is restored in the PFC cell.

An Ag-supported TiO<sub>2</sub> (Ag–TiO<sub>2</sub>) sample was calcined at 673 K. The color was light yellow, which indicated the presence of metallic Ag.<sup>0,20</sup> However, the color changed to purple in air after 24 h (Fig. 1A). The silver K-edge extended X-ray absorption fine structure (EXAFS, Fig. 1B–a) demonstrated the dominance of Ag<sub>2</sub>O based on the interatomic pair of Ag and O at 0.2305 nm by curve-fit analysis (Table S1a, ESI†). Scanning electron microscopy (SEM, Fig. 2A), transmission electron microscopy (TEM, Fig. 2B) and high-resolution

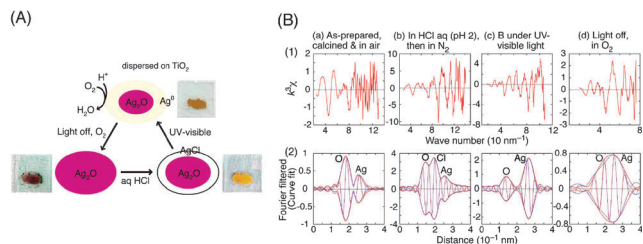


**Fig. 1** (A) Transformation of Ag active sites on the Ag-TiO<sub>2</sub> photocatalyst. (B) (a) Silver K-edge EXAFS spectra of as-prepared Ag-TiO<sub>2</sub> (3.0 wt%-Ag), (b) sample a was immersed in a HCl solution of pH 2.0 and then kept under 101 kPa of N<sub>2</sub>, (c) sample b was irradiated under UV-visible light, and (d) the light was turned off and sample c was kept under 101 kPa of O<sub>2</sub>. Note that (1) corresponds to the *k*<sup>3</sup>-weighted EXAFS  $\chi$ -function and (2) corresponds to best-fit results in *R*-space to the Fourier-filtered transformed data. The red line represents the experimental values, and the blue line represents calculated values. The solid line represents the magnitude and the dotted line represents the imaginary part in panel (2).

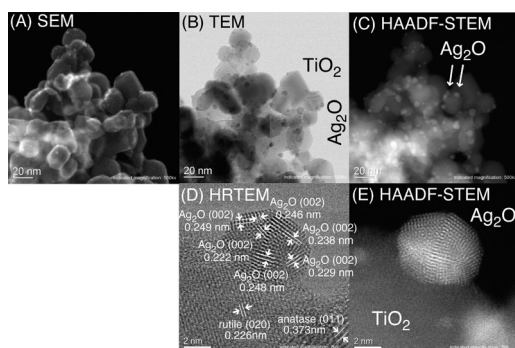


**Fig. 2** SEM (A), TEM (B), HR-TEM (D), and HAADF-STEM images (C, E) of as-prepared Ag-TiO<sub>2</sub> photocatalysts stored in ambient air.

(HR) TEM (Fig. 2D) images revealed Ag<sub>2</sub>O nanoparticles with a mean size of 3.8 nm accompanying lattice intervals between 0.222 and 0.249 nm, corresponding to the (002) lattice ( $a/2 = 0.2361$  nm) and not the (111) lattice ( $a/\sqrt{3} = 0.2726$  nm).<sup>21</sup> The brightness of the high angle annular dark field (HAADF)-scanning TEM (STEM) image was proportional to the square of atomic weight and distinguished <sub>47</sub>Ag and <sub>22</sub>Ti atoms (Fig. 2C and E). Indeed, the distribution of Ag<sub>2</sub>O nanoparticles on TiO<sub>2</sub> was clearly observed (Fig. 2C), and the atomic resolution image of a single Ag<sub>2</sub>O nanoparticle supported the presence of Ag<sub>2</sub>O (Fig. 2E), as shown in the HR-TEM image (Fig. 2D). A weak peak due to the interatomic pair of Ag and Ag because of metallic Ag<sup>0</sup> was also observed by EXAFS (Fig. 1B-a2); however, the population was small ( $\sim 10\%$  on atom basis) based on the curve-fit analysis (Table S1a, ESI<sup>†</sup>).

The photocurrent generation of PFC comprising TiO<sub>2</sub> and Ag-TiO<sub>2</sub>, both placed on an indium tin oxide (ITO)-coated Pyrex glass electrode, was tested under N<sub>2</sub> and O<sub>2</sub> gas flows, respectively, separated by a PCP film. When the Ag-TiO<sub>2</sub> film on the electrode was immersed in a HCl solution with a pH of 2.0, the color of the film changed to light yellow within 5 s (Fig. 1A, right). The interatomic pair distance between Ag and Cl at 0.262 nm obtained by EXAFS (Fig. 1B-b2 and Table S1b, ESI<sup>†</sup>) demonstrated that outer layers of Ag<sub>2</sub>O transformed to colorless Ag(I) chloride (Fig. 1A, right). The light yellow color was due to the small number of inert Ag<sup>0</sup> nanoparticles.

When the Ag-TiO<sub>2</sub> on the electrode immersed in a HCl solution at a pH of 2.0 was irradiated by UV-visible light, the yellow color changed to ochre within 10 s (Fig. 1A, top). From the EXAFS data, it was observed that the interatomic pair of Ag and Ag became predominant and the distance was 0.287 nm (Fig. 1B-c2 and Table S1c, ESI<sup>†</sup>). Therefore, all of the outer layer AgCl and a part of the inner layer Ag<sub>2</sub>O were transformed to metallic yellow Ag<sup>0</sup> due to the reduction by photogenerated electrons diffused from TiO<sub>2</sub>.<sup>20</sup>

In response to the UV-visible irradiation, the photocurrents increased and stabilized within 6–9 min at pH 3.0 (Fig. 3A1). In five light on-off cycles, the photocurrents converged to 11.8–12.7, 17.6–18.8, and 26.0–26.7  $\mu$ A using Ag-TiO<sub>2</sub> of 0.33, 1.0, and 3.0 wt%-Ag, respectively, on a photocathode. The converged photocurrent values were plotted as a function of the Ag content in the Ag-TiO<sub>2</sub> photocatalysts (Fig. 3A2), and they increased proportionally to the cube root of the Ag content.

Next, the dependence of photocurrents on the pH of the electrolyte solution was investigated for the PFC comprising TiO<sub>2</sub> and Ag-TiO<sub>2</sub> (3.0 wt% of Ag) at the pH values between 2.0 and 4.0 (Fig. 3B1, 2). Throughout this study, the pH values changed negligibly (within the variation of 0.02) over 5 h. The photocurrents stabilized within 1–11 min of irradiation and converged to 26.0–26.7  $\mu$ A at pH 3.0. The current gradually increased from 43.7 to 60.5  $\mu$ A in five cycles at pH 2.0 (Fig. 3B1); in contrast, the current gradually decreased from 3.2 to 2.6  $\mu$ A at pH 4.0 (B2). The photocurrents quickly decreased to zero over 6 min at pHs of 2.0 and 3.0 when the UV-visible light was off, while the currents decreased more slowly (30–43 min) at pH 4.0. This suggested limited diffusion at lower proton concentrations. The converged PFC photocurrent values were plotted as a function of electrolyte solution proton concentrations (Fig. 3B3).

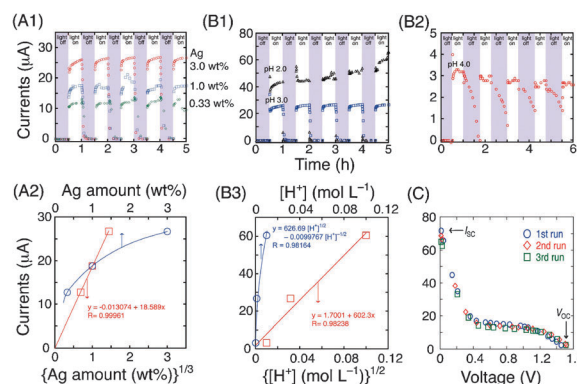


**Fig. 3** (A1) The time course of photocurrents of the PFC comprising TiO<sub>2</sub> and Ag-TiO<sub>2</sub> photocatalyst electrodes immersed in a HCl solution at pH of 3.0. Circle (○): 3.0 wt% of Ag, square (□): 1.0 wt% of Ag, and diamond (◇): 0.33 wt% of Ag for Ag-TiO<sub>2</sub>. (A2) The correlation between converged photocurrents within 5 h and the amount of Ag (wt%) or cube root of the amount of Ag and the fits. (B1, 2) The time course of photocurrents in the PFC comprising TiO<sub>2</sub> and Ag-TiO<sub>2</sub> (3.0 wt%-Ag) photocatalyst electrodes, which are immersed in a HCl solution at pH 2.0 (triangle, Δ), 3.0 (square, □) (B1), and 4.0 (circle, ○) (B2). (B3) The correlation between converged photocurrents within 5 h and the H<sup>+</sup> concentrations of acid solution in the PFC or the power of square of the H<sup>+</sup> concentrations. The fits were to linear function (lower x-axis) or to the kinetic model equation  $i = A[H^+]_c^{1/2} - B[H^+]_c^{-1/2}$  (eqn (2), see text; upper x-axis). (C) *i*-*V* dependence for PFC comprising TiO<sub>2</sub> and Ag-TiO<sub>2</sub> (3.0 wt%-Ag) immersed in a HCl solution at pH 2.0.

The values increased proportionally to the square root of the proton concentrations.

The current ( $i$ )-voltage ( $V$ ) characteristic was also studied for the TiO<sub>2</sub> and Ag-TiO<sub>2</sub> of 3.0 wt%-Ag PFC at pH 2.0 (Fig. 3C). The  $i$  value gradually increased as the cell voltage decreased, starting from the open circuit voltage ( $V_{OC}$ , 1.59 V), which is similar to the  $i$ - $V$  dependence for the SCs.<sup>22</sup> When the voltage was less than 0.45 V, the current increased linearly from 20 to 74  $\mu$ A (short circuit current,  $I_{SC}$ ). The maximum electric power was 14  $\mu$ W ( $1.1$  V  $\times$  13  $\mu$ A) among the three runs using the photocatalyst film area of 1.3 cm<sup>2</sup>. As a comparison test, Ag mesh (150  $\mu$ m- $\phi$ , 40 lines in 2.54 cm) was used as an electrode instead of ITO-coated glass. The  $V_{OC}$  (0.52 V) and  $I_{SC}$  (107  $\mu$ A) obtained for PFC using Ag mesh were quite different from that obtained using ITO-coated glass (1.59 V, 74  $\mu$ A; Fig. 3C), suggesting that the interface between photocatalysts and electrodes (In/Sn oxide, Ag) was also critical for the characteristic of PFC.

The  $i$ - $V$  characteristic can be explained based on the equivalent SC circuit comprising a diode, a series resistance ( $R_{series}$ ), and a shunt resistance ( $R_{shunt}$ ).<sup>23</sup> The current  $i$  can be expressed as follows

$$i = i_{photo} - i_{diode} \left[ \exp\left(\frac{e(V + iR_{series})}{nkT}\right) - 1 \right] - \frac{V + iR_{series}}{R_{shunt}} \quad (1)$$

where  $i_{photo}$  is the photoelectric current,  $i_{diode}$  is saturated  $i$  of the diode,  $n$  is a constant for the diode,  $e$  is elementary charge,  $k$  is Boltzmann constant, and  $T$  is the temperature of the cell. The  $R_{series}$  and  $R_{shunt}$  values were calculated to be 35 and 5.9 k $\Omega$  cm<sup>2</sup>, respectively, based on the tangent lines from  $V_{OC}$  and  $I_{SC}$  (Fig. 3C). Compared to the general requisite for ideal Si SCs ( $R_{series} < 1$   $\Omega$  cm<sup>2</sup>,  $R_{shunt} > 1$  k $\Omega$  cm<sup>2</sup>), the resistance in photocatalysts and that at the interface between photocatalysts and electrodes needs to be improved for PFCs to decrease the  $R_{series}$  value.

The PFC photocurrents are generated by the balance of photoexcitation and charge recombination in TiO<sub>2</sub> and Ag-TiO<sub>2</sub> photocatalysts, and the reaction rates of water photooxidation and O<sub>2</sub> photoreduction (Scheme 1) analogous to dye-sensitized SCs, in which the dye attached to TiO<sub>2</sub> is photooxidized and the redox mediator is reduced at the cathode.

The allowed indirect band gap electronic transition<sup>24</sup> leads to the separation of electrons and holes in TiO<sub>2</sub>. The equilibrium constants of charge separation ( $K_a$  and  $K_c$ ) are assumed in the photoanodic TiO<sub>2</sub> and photocathodic Ag-TiO<sub>2</sub>, respectively. The electrons excited to CB for Ag-TiO<sub>2</sub> may be favorably trapped at the Ag sites<sup>20</sup> owing to the Schottky barrier (work functions: 4.52–4.74 eV (Ag)<sup>25</sup> > 4.13–4.3 eV (TiO<sub>2</sub>)<sup>26,27</sup>). The trap was evidenced by the reduction of Ag<sup>I</sup> to Ag<sup>0</sup> in EXAFS for Ag-TiO<sub>2</sub> immersed in a HCl solution and irradiated by UV-visible light (Fig. 1B-c and Table S1c, ESI†).

The photooxidation over TiO<sub>2</sub> was essentially irreversible under the N<sub>2</sub> flow. The rate and rate constant were denoted as  $r_{ox}$  and  $k_{ox}$ , respectively. The O<sub>2</sub> photoreduction at Ag-TiO<sub>2</sub> was in equilibrium with the product (water) and the constant is denoted as  $K_{red}$ . The forward electron flow rate from TiO<sub>2</sub> to Ag-TiO<sub>2</sub> *via* the external circuit should be proportional to both the excited electron concentration in TiO<sub>2</sub> and the hole Ag-TiO<sub>2</sub> concentration based on the principle of PFC as shown in Scheme 1. The reverse electron flow rate should be proportional to both the unreacted trapped electron concentration at Ag-TiO<sub>2</sub> and the unreacted hole concentration

at TiO<sub>2</sub>. Thus, the effective electron flow rate (photocurrent  $i$ ) is formulated in eqn (2). The derivation is shown in eqn (S1)–(S4) (ESI†).

$$i = k \frac{K_a' (k_{ox}')^{\frac{1}{4}} (K_c')^{\frac{1}{2}} (K_{red}')^{\frac{1}{8}} ([O_2]_c)^{\frac{1}{8}} ([H^+]_c)^{\frac{1}{2}}}{(r_{ox}')^{\frac{1}{4}}} - k' \frac{(r_{ox}')^{\frac{1}{4}} (K_c')^{\frac{1}{2}}}{(k_{ox}')^{\frac{1}{4}} (K_{red}')^{\frac{1}{8}} ([O_2]_c)^{\frac{1}{8}} ([H^+]_c)^{\frac{1}{2}}} \quad (2)$$

where [O<sub>2</sub>] and [H<sup>+</sup>] with a subscript “c” denote the concentrations of O<sub>2</sub> and H<sup>+</sup> in acidic solution around the cathode, and rate and equilibrium constants with the prime symbol denote the constants multiplied with essentially constant concentrations for predominant species in acidic solution/photocatalysts (see ESI† for a detailed definition).

The experimental data fit of pH dependence in eqn (2) is presented in Fig. 3B3 per  $x$ -axis. The second term was negligible in the fit ( $i = 626.7 [H^+]^{1/2} - 0.009977 [H^+]^{-1/2}$ ), demonstrating that the reverse electron flow from Ag to the VB of anodic TiO<sub>2</sub> *via* external circuit was minimal. Moreover, the net photocurrents were essentially proportional to [H<sup>+</sup>]<sup>1/2</sup> (Fig. 3B3, lower  $x$ -axis; the first term of eqn (2)). In this study, PFC was advantageous for rectifying the electron flow direction owing to the Schottky barrier between TiO<sub>2</sub> and Ag nanoparticles. Moreover, the suppression of the reverse reaction at anodic TiO<sub>2</sub> by purging the resultant O<sub>2</sub>, analogous to the suppression of dye re-reduction by electron transfer from the CB of TiO<sub>2</sub> to the dye in dye-sensitized SC.<sup>22</sup> In addition, the total current generated as shown in Fig. 3B1 (pH 2.0) corresponded to 4.9  $\mu$ mol- $e^-$  *versus* the amount of Ag mounted on the cathode which was 1.4  $\mu$ mol. Therefore, major part of the forward electron flow to Ag on cathode should be consumed to reduce O<sub>2</sub>.

The effects of Ag (electron trap and electron transfer to O<sub>2</sub>-derived species) are related to the charge separation equilibrium  $K_c$  (or  $K_c' = K_c [Ag^+]_d [O_2^-]_c$ , ESI†) that appears in eqn (2). The weight ( $w$ ) of sphere-like Ag nanoparticles (Fig. 2) is proportional to the cube of the average radius ( $w = N \frac{4}{3} \pi (\bar{r})^3 \rho$ , where  $N$  is the number of Ag nanoparticles and  $\rho$  is the density). The effective charges trapped in Ag for photocatalysis should be related to the surface area of Ag nanoparticles,  $4N\pi(\bar{r})^2 = (4N\pi)^{\frac{2}{3}} (3w/\rho)^{\frac{2}{3}}$ . The dependence of effectively trapped charges on  $w$  (2/3) takes into account the square root dependence of the first term in eqn (2) on  $K_c'$  ( $2/3 \times 1/2 = 1/3$ ). Thus, the cube root dependence of photocurrents on the Ag content (Fig. 3A2) can also be explained.

In the cyclic voltammetry (CV) measurements for Ag-TiO<sub>2</sub> (3.0 wt% of Ag) in an aqueous HCl solution of pH 4.0, only the redox reactions of AgCl ( $AgCl + e^- \rightleftharpoons Ag^0 + Cl^-$ ) and H<sub>2</sub> formation ( $2H^+ + 2e^- \rightarrow H_2$ ) occurred under N<sub>2</sub> in the dark (Fig. 4d and Table S2, ESI†). When the Ag-TiO<sub>2</sub> was irradiated by UV-visible light, the redox reactions of Ag<sub>2</sub>O ( $Ag_2O + 2H^+ + 2e^- \rightleftharpoons 2Ag^0 + H_2O$ ) also occurred (Fig. 4c). Under O<sub>2</sub>, the reduction reaction peak from Ag<sub>2</sub>O to Ag<sup>0</sup> at 0.35 V (*versus* SHE) was more intense, as seen in Fig. 4a, when irradiated by UV-visible light compared to Fig. 4b, which shows the reduction peak in the dark. This result is in accordance with the Ag photoreduction as monitored using EXAFS (Fig. 1B-c). If the photoreduction of Ag is coupled with simple oxidation of Ag by O<sub>2</sub>

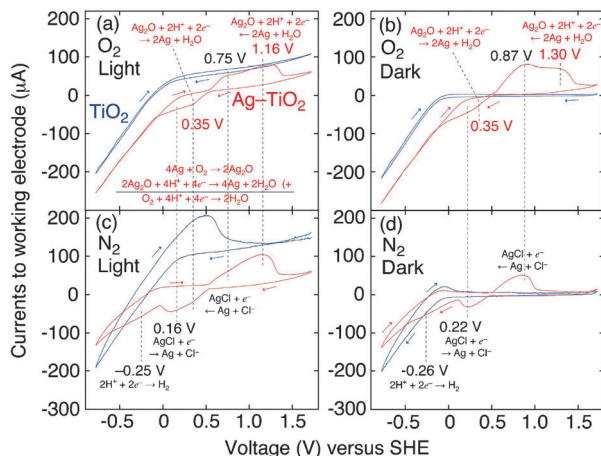


Fig. 4 CV for the TiO<sub>2</sub> or Ag–TiO<sub>2</sub> (3.0 wt% of Ag) working electrode and the glassy carbon counter electrode in an aqueous HCl solution of pH 4.0 under an O<sub>2</sub> flow (a, b) or N<sub>2</sub> flow (c, d) under the irradiation by UV-visible light (a, c) or in the dark (b, d).

(4Ag + O<sub>2</sub> → 2Ag<sub>2</sub>O), O<sub>2</sub> photoreduction at the cathode of the PFC can be explained (Fig. 4a, bottom inset, chemical formula). In contrast, no distinct peaks appeared under any of the conditions employed for TiO<sub>2</sub>.

The feasibility of PFCs comprising two photoelectrodes was demonstrated using TiO<sub>2</sub> and Ag–TiO<sub>2</sub> immersed in a HCl solution of pH 2, separated by a PCP film. The V<sub>OC</sub>, I<sub>SC</sub>, and maximum power were 1.59 V, 74 μA, and 14 μW, respectively. TiO<sub>2</sub> photooxidized water under a N<sub>2</sub> flow, while Ag–TiO<sub>2</sub> photoreduced O<sub>2</sub>. The kinetic model successfully explained the photocurrent dependences on pH values and the amount of Ag. The quantum efficiency was evaluated to be 20% both for photooxidation and photoreduction (ESI<sup>†</sup>) and that of PFC should be the product (4%). The quantum efficiency needs to be improved by the optimization of photocatalysts on the cathode and the thickness, packed density, and the serial resistance for photocatalysts on electrodes.

The authors are grateful for the financial support from the Feasibility Study Stage of A-STEP (AS251Z00906L, AS231Z01459C) from the Japan Science and Technology Agency, the Iwatani Naoji Foundation (2011–2012), and the Grant-in-Aid for Scientific Research C (22550117) from MEXT (2010–2012). X-ray absorption

experiments were conducted under the approval of the Photon Factory Proposal Review Committee (2013G159).

## Notes and references

- 1 N. S. Lewis and D. G. Nocera, *Proc. Natl. Acad. Sci. U. S. A.*, 2006, **103**, 15729.
- 2 Y. Izumi, *Coord. Chem. Rev.*, 2013, **257**, 171.
- 3 J. R. Bolton, *Sol. Energy*, 1996, **57**, 37.
- 4 M. Grätzel, *Nature*, 2001, **414**, 338.
- 5 H. A. Gasteiger and N. M. Marković, *Science*, 2009, **324**, 48.
- 6 K. S. Joya, Y. F. Joya, K. Ocakoglu and R. van de Krol, *Angew. Chem., Int. Ed.*, 2013, **52**, 10426.
- 7 X. Chen and S. S. Mao, *Chem. Rev.*, 2007, **107**, 2891.
- 8 N. Serpone, *J. Phys. Chem. B*, 2006, **110**, 24287.
- 9 H. B. Gray, *Nat. Chem.*, 2009, **1**, 7.
- 10 J. K. Hurst, *Science*, 2010, **328**, 315.
- 11 K. Li, Y. Xu, Y. He, C. Yang, Y. Wang and J. Jia, *Environ. Sci. Technol.*, 2013, **47**, 3490.
- 12 P. Lianos, *J. Hazard. Mater.*, 2011, **185**, 575.
- 13 B. D. Alexander, P. J. Kulesza, I. Rutkowska, R. Solarska and J. Augustynski, *J. Mater. Chem.*, 2008, **18**, 2298.
- 14 K. Ren, Y. X. Gan, T. J. Young, Z. M. Moutassem and L. Zhang, *Composites, Part B*, 2013, **52**, 292.
- 15 K. Ren, C. A. McConnell, Y. X. Gan, A. A. Afjeh and L. Zhang, *Electrochim. Acta*, 2013, **109**, 162.
- 16 C. Leygraf, M. Hendewerk and G. A. Somorjai, *J. Phys. Chem.*, 1982, **86**, 4484.
- 17 K. Sayama, K. Mukasa, R. Abe, Y. Abe and H. Arakawa, *Chem. Commun.*, 2001, 2416.
- 18 K. Fujihara, T. Ohno and M. Matsumura, *J. Chem. Soc., Faraday Trans.*, 1998, **94**, 3705.
- 19 Q. Chen, J. Li, X. Li, K. Huang, B. Zhou, W. Cai and W. Shangguan, *Environ. Sci. Technol.*, 2012, **46**, 11451.
- 20 M. K. Seery, R. George, P. Floris and S. C. Pillai, *J. Photochem. Photobiol., A*, 2007, **189**, 258.
- 21 Predominance of (002) lattices suggested that the Ag<sub>2</sub>O particle in Fig. 2D and E was polycrystalline rather than a single crystal.
- 22 A. Y. Anderson, P. R. Barnes, J. R. Durrant and B. C. O'Regan, *J. Phys. Chem. C*, 2011, **115**, 2439.
- 23 K. Bouzidi, M. Chegaar and A. Bouhemadou, *Sol. Energy Mater. Sol. Cells*, 2007, **91**, 1647.
- 24 Y. Izumi, T. Itoi, S. Peng, K. Oka and Y. Shibata, *J. Phys. Chem. C*, 2009, **113**, 6706.
- 25 R. C. Weast, *CRC Handbook of Chemistry and Physics*, CRC Press, Boca Raton, USA, 2001, vol. 82, pp. 12–130.
- 26 A. Imanishi, E. Tsuji and Y. Nakato, *J. Phys. Chem. C*, 2007, **111**, 2128.
- 27 D. O. Scanlon, C. W. Dunnill, J. Buckeridge, S. A. Shevlin, A. J. Lodsail, S. M. Woodley, R. A. Catlow, M. J. Powell, R. G. Palgrave, I. P. Parkin, G. W. Watson, T. W. Keal, P. Sherwood and A. A. Sokol, *Nat. Mater.*, 2013, **12**, 798.